

# Holistic Interpretation of Public Scenes Using Computer Vision and Temporal Graphs to Identify Social Distancing Violations

Gihan Jayatilaka<sup>a,b,1</sup>, Jameel Hassan<sup>a,1,\*</sup>, Suren Sritharan<sup>c,d,1</sup>, Janith Bandara Senanayaka<sup>a</sup>, Harshana Weligampola<sup>a</sup>, Roshan Godaliyadda<sup>a</sup>, Parakrama Ekanayake<sup>a</sup>, Vijitha Herath<sup>a</sup>, Janaka Ekanayake<sup>a</sup>, Samath Dharmaratne<sup>f</sup>

<sup>a</sup>Department of Electrical and Electronic Engineering, University of Peradeniya

<sup>b</sup>Department of Computer Science, University of Maryland

<sup>c</sup>School of Computing and IT, Sri Lanka Technological Campus

<sup>d</sup>Department of Informatics, Technical University of Munich

<sup>e</sup>School of Engineering, Cardiff University

<sup>f</sup>Department of Community Medicine, University of Peradeniya

---

## Abstract

Social distancing measures are proposed as the primary strategy to curb the spread of the COVID-19 pandemic. Therefore, identifying situations where these protocols are violated, has implications for curtailing the spread of the disease and promoting a sustainable lifestyle. This paper proposes a novel computer vision-based system to analyze CCTV footage to provide a threat level assessment of COVID-19 spread. The system strives to holistically interpret the information in CCTV footage spanning multiple frames to recognize instances of various violations of social distancing protocols, across time and space, as well as identification of group behaviors. This functionality is achieved primarily by utilizing a temporal graph-based structure to represent the information of the CCTV footage and a strategy to holistically interpret the graph and quantify the threat level of the given scene. The individual components are evaluated on a range of scenarios and the complete system is tested against human expert opinion. The results reflect the dependence of the threat level on people, their physical proximity, interactions, protective clothing, and group dynamics. The system performance has 76% accuracy, enabling a deployable threat monitoring system in cities, permitting sustainable normalcy in society.

*Keywords:* COVID-19, Computer vision, surveillance, artificial intelligence

---

## 1. Introduction

The COVID-19 is a viral infection that causes a wide range of complications, primarily in the respiratory system [1] along with other systems [2, 3]. As per current statistics, even though the virus has a comparatively small case mortality rate, it has amassed a massive fatality count due to its high infectiousness. The World Health Organization (WHO) estimates that the virus has infected around 338

---

\*Correspondence: Jameel Hassan, Department of Electrical and Electronic Engineering, University of Peradeniya, Peradeniya 20400, Sri Lanka. jameel.hassan.2014@eng.pdn.ac.lk

<sup>1</sup>Equally contributing authors listed in the alphabetical order of last names.

million people and claimed more than 5.72 million lives as of December 2021. Despite the availability of effective vaccines against virus spread, medical complications and mortality; complete global vaccination coverage is still far due, owing to vaccine production, distribution, and other logistic and regulatory issues. Furthermore, emerging variants cast some non-trivial obstacles for vaccine efficiency [4, 5, 6, 7]. Therefore, mitigating the spread of the disease through social distancing, mask-wearing, hand washing, sanitizing, and other practices of hygiene still remains indispensable by and large [8, 9] to restore normalcy whilst ensuring safety of health.

As such, non-pharmaceutical interventions (NPI) are still essential for the effective containment of COVID-19 even with vaccination roll-out. NPI techniques refer to measures that people can take, to reduce the opportunities for the spread of the pandemic. COVID-19 spreads through droplet [10] and aerosol [11, 12] transmission and therefore, the recommended NPI for containment is primarily social distancing. Social distancing is the behaviour of minimizing physical distance with each other, while refraining from touching potentially contaminated items/surfaces, and wearing face masks. Studies in [13, 14, 15] have proven that maintaining interpersonal distances of more than 1m reduces the spread of COVID-19 by 75%. Furthermore, [16, 17] have shown that avoiding physical interactions between people can drastically reduce the spread, while [18] depicts the importance of wearing masks to mitigate the spread of COVID-19.

People, being a social species, tend to exhibit group behaviors frequently. Therefore, even the most mindful persons may violate social distancing protocols occasionally [19, 20]. Even such occasional violation of social distancing protocols may garner a risk of contracting COVID-19 depending on the proximity or duration of the violation [21, 22]. Conversely, monitoring such violations of social distancing protocols (i.e. proximity, duration as well as the intensity of sudden events such as maskless cough or sneezing) provide vital tools for contact tracing, monitoring, and eventually pandemic control. Nevertheless, if a certain set of individuals remain in a group throughout an observation window, then whatever interaction during that observation window, has no impact on the potential of contracting COVID-19 within the group — hence commonly known as a “bio-bubble” or simply a “bubble”. In essence, observing social distancing protocol violations is a task with many caveats. Thus, such monitoring is tedious to do manually, whereas automating such a task needs meticulous analysis [23]. The main two avenues of research have been (a) intrusive solutions where people are actively contributing to the measurement (by handheld devices etc.) and (b) non-intrusive solutions with zero burden on the people (which could be deployed to any situation irrespective of who is being monitored).

The first type (intrusive techniques) requires a signal to be transmitted by the people being tracked, i.e. methods of this type requires a active beacon by each tracked person. The information extracted from the analysis of these signals can be either absolute locations of people (which could be used to calculate the distances between individuals) or relative positions (which itself is indicative of the social

distancing situation). Such a wearable device based on an oscillating magnetic field for proximity sensing to monitor social distancing to prevent COVID-19 has been presented in [24]. This system was shown to be more robust than Bluetooth sensing devices [25], especially in determining the distance threshold limit. However, it is practically difficult to deploy a solution of this type in a public space in a real-world situation. Thus, a non-intrusive solution is preferable for large-scale deployment in public spaces as the people who are being tracked are done so passively.

Research in non-intrusive techniques to monitor social distancing has led to a large body of work utilizing computer vision techniques. The major sub-tasks in those approaches are detection and tracking of people and the state of the art for these sub-tasks are now primarily dominated by convolution neural networks (CNNs), which is a type of artificial neural networks (ANN). The detection and localization task together is achieved by region proposal networks such as RCNNs [26], Single Shot Detection (SSD) [27], and YOLO [28] which operate on individual frames. After identifying objects in each frame, tracking is done on a sequence of frames by classical methods such as Kalman filtering [29], particle filtering [30] or modern methods such as SORT [31] and deepSORT [32]. Most recent applications combine YOLO and deepSORT to form powerful tools which can achieve object detection and tracking in real-time and it is used to tackle object recognition problems in different scenarios such as license plate recognition [33], road marking detection [34], pedestrian detection [35], and agricultural production [36], etc.

The work in [37] is an example of a CNN framework built on the aforementioned detection and localization algorithms to detect people, calculate Euclidean distance between them and spot social distancing violations. A similar approach using YOLOv3 is performed in [38, 39] for birds-eye view (overhead) camera footage. However, such overhead viewpoints are not practically deployable in public settings. An SSD-based model is presented in [40], which also performs person detection and social distancing violation identification. The performance is compared for each of the deep learning models Faster RCNN, SSD, and YOLO. Reference [41] utilizes the YOLOv4 model for people detection in low light instances to enforce social distancing measures. In [42], a spatio-temporal trajectory-based social distancing measurement and analysis method is proposed. This problem has been further examined in [43, 44, 45].

While various solutions proposed in the literature strives to assess the adherence to social distancing protocols, they fall short of incorporating factors such as mask-wearing, critical to the current COVID-19 pandemic. The presence or absence of a mask on a person greatly affects the efficacy of the social distancing protocols [18]. Similarly, inter-person interactions such as hugs, kisses, and handshakes are severe concerns than mere distancing amongst individuals [16, 17] as far as the person-to-person spreading of COVID-19 is concerned. The detection of mask-wearing [46, 47, 48, 49] as well as the detection of dyadic interactions [50, 51, 52] have been explored in computer vision as isolated and distinct problems. However, to the best of the knowledge of the authors, those factors have not been incorporated into

a unified and holistic solution for detecting violations of social distancing protocols in the literature. Ignoring such factors vastly undermines the robustness of vision-based techniques to tackle the social distancing problem for COVID-19.

In this light, the system proposed in this paper analyzes the spatial and temporal interactions manifested over multiple frames. A single frame was analysed to recognize how people adhere to social distancing measures such as keeping proper distance, mask-wearing, and handshake interactions. The risk of spreading COVID-19 increases when an individual interacts with multiple people, and the nature of the interaction. On the other hand, if a certain set of people are in a “bubble” and they remain so until the end of observation, there is no change in the risk of spreading COVID-19. This temporal analysis of identifying bio-bubbles is also included in our proposed model.

In this paper, the design, implementation and testing of a complete end-to-end system comprising of a framework to fit in different computer vision and deep learning based techniques, a representation to store the output of the deep learning models, and an interpretation technique to evaluate the threat level of a given scene are discussed. The key contributions of this paper are as follows:

- A deep learning based system to monitor social distancing violations and COVID-19 threat parameters. The system can utilize multiple computer vision modules to extract different information from the video sequence such as the number of people, their location, their physical interactions, and whether they wear masks.
- A temporal graph representation to structurally store the information extracted by the computer vision modules. In this representation, people are represented by nodes with time-varying properties for their location and behavior. The edges between people represent the interactions and social groups.
- A methodology to interpret the graph and quantify the threat level in every scene based on primary and secondary threat parameters such as individual behavior, proximity and group dynamics extracted from the graph representation.
- A novel approach for dyadic human interaction detection and localization in a multiple-person setting.

## **2. Proposed solution**

This section explains the graph-based computer vision framework proposed to quantify the risk of COVID-19 transmission in various public scenarios. The input video feed from closed circuit television (CCTV) footage is first used to extract key information such as people, handshake interactions, and face masks through computer vision models. The proposed system then quantifies the risk of transmission of COVID-19 by encoding the extracted information into a temporal graph and interpreting it using

a function for threat of transmission developed in this paper. An overview of the proposed system is depicted in Fig. 1.

The system takes a video stream  $V_{in}(t)$  as the input, where  $t$  denotes the frame number. The video stream is considered to be captured from a CCTV system camera mounted at a desired vantage point with a known frame rate.  $V_{in}(t)$  is a three-dimensional matrix with the dimensions  $H \times W \times 3$ , where  $H$  and  $W$  denote the frame's height and width, respectively.

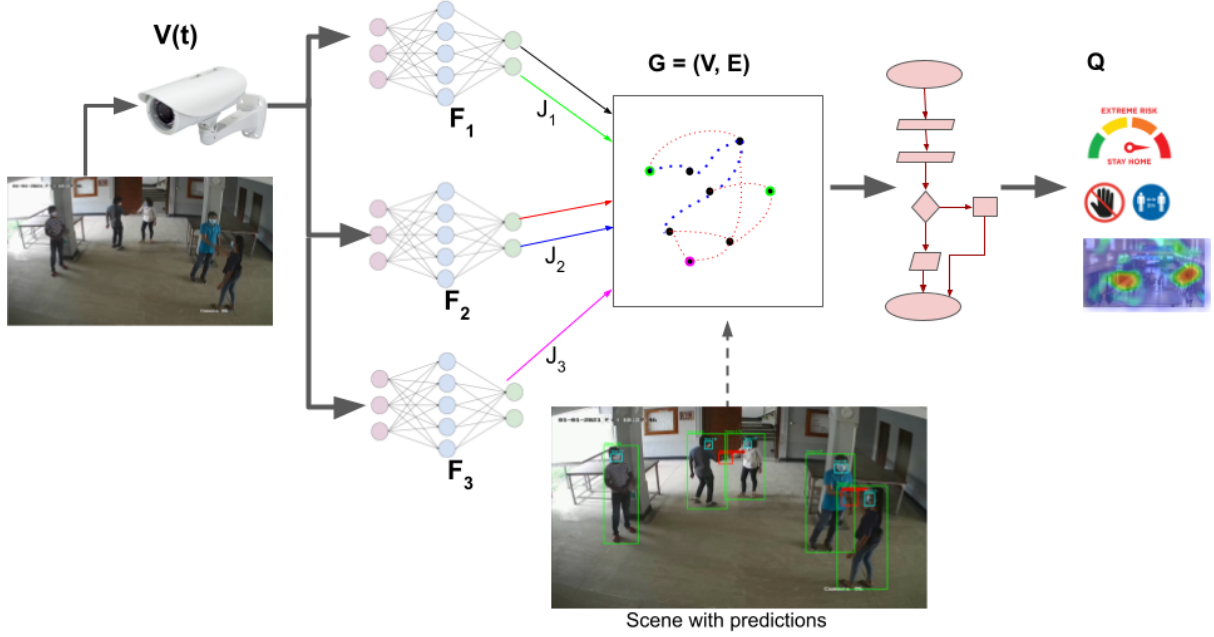


Figure 1: A high-level overview of the proposed system

The video feed,  $V_{in}(t)$ , was passed into a series of functions  $F_i$ ;  $i \in \{p, d, g, h, m\}$ . Each  $F_i$  processes a video frame and produces different information as,

$$J_i(t) = F_i(V_{in}(t)) \quad (1)$$

where  $J_i(t)$  denotes an output, such as the locations of people, handshake interactions, or the presence of face masks. While the functions  $F_i$ s process individual frames, processing a sequence of frames is required to analyze this information across time. Therefore, a collection of trackers  $\overline{F}_i$  was employed to track the above-mentioned detections provided by  $F_i$ s over time as,

$$[S_i(t), \overline{J}_i(t)] = \overline{F}_i(V_{in}(t), J_i(t), S_i(t-1)) \quad (2)$$

where  $S_i(t)$  is the state and  $\overline{J}_i(t)$  is the tracking interpretations based on the sequential information.

The list of functions utilized to obtain spatial information necessary for detecting and localizing persons, interactions, and face masks are as follows:

1. People detection ( $F_p$ ) and tracking ( $\overline{F}_p$ )

2. Distance estimation ( $F_d$ ) and group identification ( $F_g$ ).
3. Identifying and localizing physical interaction (handshakes) ( $F_h$ ).
4. Mask detection ( $F_m$ ).

Table 1: Notations and description

Notation	Definition
$V_{in}(t)$	Input video feed.
$F_p, \bar{F}_p$	People detection and tracking.
$F_d$	Distance estimation.
$F_g, \bar{F}_g$	Group identification and tracking.
$F_h$	Identifying and localizing physical interaction (handshakes)
$F_m, \bar{F}_m$	Mask detection and tracking.
$J_i(t)$	Output of model $F_i$ .
$S_i(t)$	State information.
$bb_{pk}(t), bbi_{pk}(t)$	Bounding box encompassing person $k$ at time $t$ and bounding box encompassing person $k$ at time $t$ which is being tracked with their unique index.
$bb_{hk}(t), bbi_{hk}(t)$	Bounding box encompassing handshake interaction $k$ at time $t$ and bounding box encompassing handshake interaction $k$ at time $t$ which is being tracked with their unique index.
$bb_{mk}(t), bbi_{mk}(t)$	Bounding box encompassing the face of person $k$ at time $t$ and bounding box encompassing face of person $k$ at time $t$ which is being tracked with their unique index.
$u, v$	The 2D coordinates of the center of the bounding box
$h, r$	The height and aspect ratio of the bounding box.
$R, R'$	The coordinates of the reference points in the video frame and 2 dimensional floor plane respectively.
$M_T$	Transformation matrix for the perspective transform from CCTV perspective to floor plane.
$s_{(i,t)}$	Standing location of person $i$ at time $t$ in the CCTV perspective.
$floorLocation_{(i,t)}$	Standing location of person $i$ at time $t$ in the floor plane.
$dist_{(i,j,t)}$	Distance between a pair of people $i$ and $j$ at time $t$ .
$P_i$	Person $i$ in the frame.
$G(t)$	Graph at time $t$
$V(t)$	Vertices of graph $G$ at time $t$ given by $\{v_1(t), v_2(t), \dots, v_n(t)\}$ , each vertex corresponding to person $P_i$ with the vertex parameters embedded.
$E(t)$	Edges of graph $G$ at time $t$ given by $\{e_{1,1}(t), e_{1,2}(t), \dots, e_{i,j}(t), \dots, e_{n,n}(t)\}$ , where $e_{i,j}$ is the edge between person(vertex) $i$ and $j$ .
$T(t)$	Threat level of frame at time $t$
$\mathbb{P} = \{p_d, p_h\}$	Primary parameters- set of parameters that have a direct attribute to COVID-19 transmission.
$\mathbb{Q} = \{q_g, q_m\}$	Secondary parameters- set of parameters that are relevant to COVID-19 transmission when two individuals are in close proximity.
$\epsilon_j$	Tuneable parameter dictating influence of parameter $q_j$ on overall threat level.

The information retrieved by the aforementioned functions, which is critical for calculating the social distancing violation measure, was encoded in a graph  $G = (V, E)$ , where vertices represent individuals with extracted information embedded as features and edges indicate their interactions. The sections 2.1 - 2.5 define the functionality of each system component that work together to populate the graph  $G$ , while Section 2.6 offers a full explanation of the data contained in the graph. Finally, the graph  $G$  was interpreted in the manner described in Section 2.7 in order to provide actionable insights based on the threat level analysis of the analyzed video. For ease of understanding, the notations used in this work are

listed in Table 1.

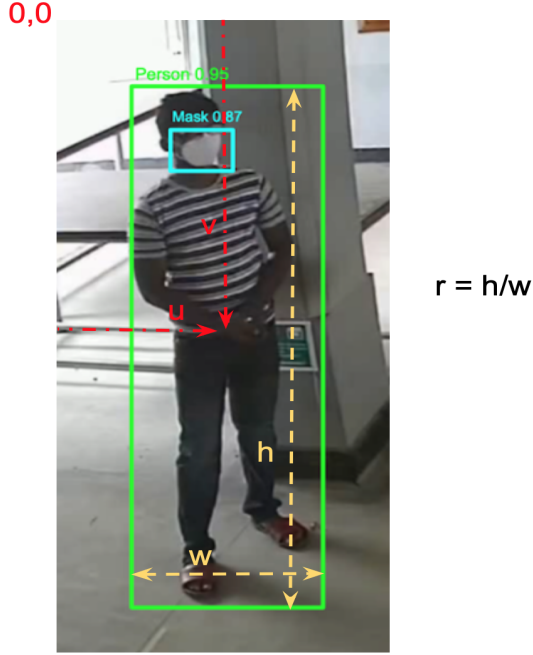


Figure 2: The parameters of the prediction for the bounding boxes

### 2.1. People detection and tracking

The detection and tracking task is the first step towards the social distancing violation problem. This section discusses the proposed framework's people detection and tracking models. The people in the scene were detected using the  $F_p$  detection model and then tracked over different frames using the  $\bar{F}_p$  tracking model. The detection model used for this purpose provides a bounding box for the person's position, whilst the tracking model assigns each person a unique ID and tracks them through time.

The detection model provides a time-varying vector containing information on people's spatial location. It is defined as  $J_p(t) = \{bb_{p1}(t), bb_{p2}(t), \dots, bb_{pk}(t), \dots, bb_{pn}(t)\}$ , where  $n$  is the number of bounding boxes and  $bb_{pk}(t) = (u, v, r, h, c_p)$  is a five-tuple that represents the bounding box representing a person at time  $t$ . In  $bb_{pk}(t)$ , variables  $u$  and  $v$  represent the two-dimensional coordinates of the bounding box's center,  $r$  represents the bounding box's aspect ratio,  $h$  represents the bounding box's height, and  $c_p$  represents the detection's confidence level, shown in Fig. 2. The tracker assigns an ID and updates bounding box information based on previous and current data. Output of the tracker is defined as  $\bar{J}_p(t) = \{bbi_{p1}(t), bbi_{p2}(t), \dots, bbi_{pk}(t), \dots, bbi_{pn}(t)\}$ , where  $bbi_{pk}(t) = (u, v, r, h, c_p, i)$  is a six-tuple representing updated bounding box information with assigned ID,  $i$ , for  $k^{\text{th}}$  person.

Given its robustness and real-time prediction capabilities, the YOLO network [53] for people detection ( $F_p$ ) and the DeepSORT algorithm [32] for tracking ( $\bar{F}_p$ ) were used in this paper. Given an image, the YOLO network predicts the bounding boxes of many predefined object classes that are present in a scene. Following that, the output  $J_1$  is created by applying non-max suppression [54] and filtering the bounding

boxes belonging to people. The DeepSORT algorithm then assigns indices,  $\overline{J}_p$ , to these detected bounding boxes using the Mahalanobis distance and the cosine similarity of the deep appearance descriptors. The publicly available weights trained using the COCO dataset [55] was used to initialize the weights of the YOLO model, whereas the weights trained using the MOT dataset [56] was used to initialize the DeepSORT model.

## 2.2. Distance estimation

The individuals identified using the detection and tracking models need to be evaluated for violations of social distancing. This section discusses the method for estimating the distance between identified individuals. The distance between people was estimated in three steps: first, by identifying the people's standing locations in the video, then by performing perspective transform and finally by measuring their Euclidean distance[57].

First, the standing locations of the people  $s_{(i,t)}$  (denoted by thick black dots in Fig. 3) were determined using the bounding box data as follows,

$$s_{(i,t)} = (u, v + 0.5h). \quad (3)$$

The standing locations were then transformed via perspective transform from an overhead wall mount camera viewpoint to a two-dimensional bird's eye viewpoint. The required transformation matrix  $M_T$  was obtained as follows,

$$\begin{aligned} R' &= M_T R \\ R' R^T &= M_T R R^T \\ R' R^T (R R^T)^{-1} &= M_T (R R^T) (R R^T)^{-1} \\ M_T &= R' R^T (R R^T)^{-1} \end{aligned} \quad (4)$$

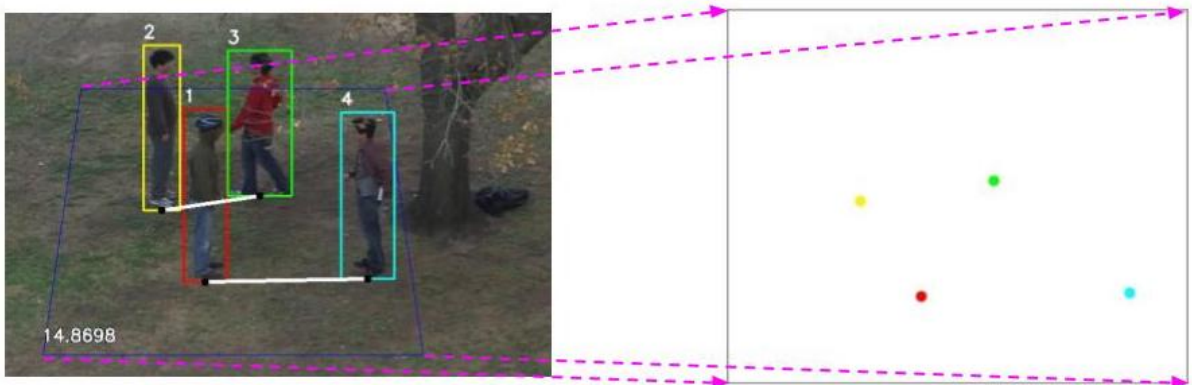


Figure 3: Perspective transformation in action. The right frame is a visualization of how a camera-captured scene (left) is projected to the 'floor plane' after perspective transform. Please note that the trapezoidal floor is being transformed into a square in this scene.



where  $R$  are  $2 \times 4$  matrices that contains the coordinates of four reference points in the video frame (refer blue trapezoid in Fig. 3 - Left) and the corresponding coordinates of those four points in the two-dimensional plane (bird’s eye view). This two-dimensional plane is referred to as the “floor plane” (refer Fig. 3 - Right). The projections was performed as,

$$floorLocation_{(i,t)} = M_T s_{(i,t)} \quad (5)$$

where  $s_{(i,t)}$  are the input coordinates from (3) and  $floorLocation_{(i,t)}$  are the output coordinates on the floor plane. Finally, the distances between each pair of people  $i$  and  $j$  in frame  $t$  were calculated as,

$$dist_{(i,j,t)} = ||floorLocation_{(i,t)} - floorLocation_{(j,t)}|| \quad (6)$$

Since the detected bounding boxes of people cannot be directly used to estimate distances between people due to the overhead camera viewing angle, the estimation is performed after perspective transform. The transform is performed based on the following assumptions. These assumptions hold for most of the scenes with a CCTV camera (including indoor premises of buildings, roads and footpaths).

1. All the people are on the same plane.
2. The camera is not a fisheye-like camera.
3. The camera is placed at an overhead level.

### 2.3. Group identification

Identifying the groups of people is an important design goal of the proposed solution, as social distancing violations within a group can be neglected. The group identification model discussed in this section utilizes the people detection, tracking and distance estimation models introduced in Sections 2.1 and 2.2. This was achieved by two algorithms  $F_g$  and  $\bar{F}_g$ .  $F_g$  was run on the information from individual frames while  $\bar{F}_g$  analyzed the results from  $F_g$  across time to properly deduce which people fall into groups based on sustained physical proximity.

Given a frame  $V_{in}(t)$ , a matrix  $M_d(t)$  called distance matrix is created based on the calculated distances between people. The affinity matrix  $M_a(t)$  was then calculated in the as follows,

$$M_a = \exp(-\alpha M_d) \quad (7)$$

where  $\alpha$  is an input parameter that is used to introduce the camera and scene pair a scale. Then, clustering was performed on  $M_a$  to split the people into clusters.

$$clusters = spectral\_clustering(M_a) \quad (8)$$

According to the group identification model, a person is considered to be a member of a group if they are closely to at least one member of the group. This is motivated by the way groups of people walk/talk. While conventional clustering algorithms attempt to minimize the distance between individual elements

and the cluster center, this is not how humans behave. As a result, this result was obtained using spectral clustering of affinity matrices [58]. Human behavior, on the other hand, cannot be analyzed in terms of discrete frames. As a result, a temporal analysis of the clusters was performed to determine the actual groups of people using a time threshold  $\tau$ . The primary idea is that a group is detected only if it persists for a specified time period  $\tau$ .

People  $P_i \in P$  being clustered from a video frame at time  $t$  as follows,

$$\text{cluster\_id}(P_i, t) \leftarrow \text{spectral\_clustering}(M_a(t)) \quad (9)$$

$$\text{cluster\_id}(P_i, t) = \text{cluster\_id}(P_j, t) \quad \text{if } \exists t_0 \text{ s.t. } t_0 \leq t \leq t_0 + \tau \quad (10)$$

where  $P_i$  and  $P_j$  were considered to be in the same social group as per Eq. (10). Social distancing violations between the people in the same social group was ignored in the proposed system as justified in Section 1. For cases involving a few people, a simplified algorithm based on naive thresholding of interpersonal distance violation occurrences was used instead of spectral clustering.

#### 2.4. Handshake interaction detection

When considering transmission in the case of COVID-19, physical interactions such as handshakes and hugs pose a greater threat. A primary design objective of the proposed system was to monitor such activity and keep track of the individuals involved for the purpose of contact tracing. Three steps were taken to detect interactions:

- Detecting and localizing physical interactions using the model in [] (citation removed for double blind purposes).
- Identifying the people involved.

The physical interactions detected in this work were handshakes, denoted by  $J_h(t)$ . Handshakes were identified using an end-to-end deep learning CNN model. The YOLO object detection model re-purposed for handshake detection combined with DeepSORT was used to detect, localize and track the handshakes. Frame level output is denoted as  $J_h(t) = \{bb_{h1}(t), bb_{h2}(t), \dots, bb_{hn}(t)\}$ , where  $n$  is the number of detected handshakes in the scene. Each bounding box  $bb_{hk}(t)$  follows the standard YOLO format specified in Section 2.1.

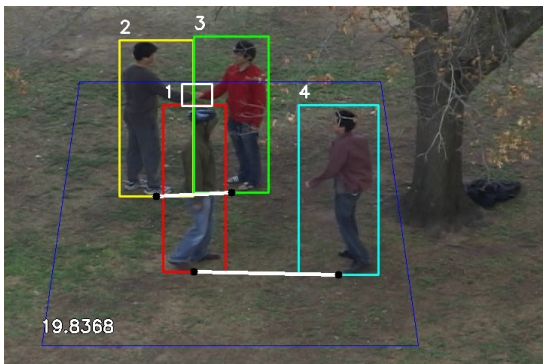
Human interaction is an action in space and time. However, the YOLO model performs detection on individual frames. Since an actual event like a handshake persists without intermittency, the interactions were considered as a sequence of frames. Therefore, DeepSORT algorithm was used to track the handshakes, which gives an output  $\overline{J}_h(t) = \{bbi_{p1}(t), bbi_{p2}(t), \dots, bbi_{pk}(t), \dots, bbi_{pn}(t)\}$ , where  $bbi_{pk}(t) = (u, v, r, h, c_p, i)$  is a six-tuple representing updated bounding box information with assigned ID,  $i$ , for  $k^{\text{th}}$  person. This maintained consistency in detecting a handshake without switching indexes between each frame.

Finally, because the detection and localization model is restricted to handshake interactions, it is necessary to identify the individuals involved in those interactions. This was accomplished by calculating the intersection over union (IoU) between handshake and person bounding boxes. The two individuals involved in a handshake are identified by the two bounding boxes of the person with the highest IoU for that handshake.

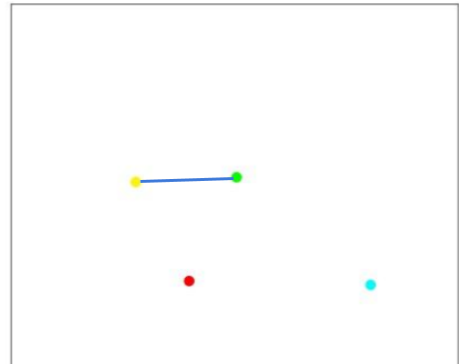
### 2.5. Mask detection

The use of masks is critical in the case of COVID-19 due to the virus’s aerosol transmission. This section describes the model used to detect the presence/absence of masks. The framework’s mask recognition stage entails identifying and tracking the presence (or absence) of masks. The model used for this purpose computes the bounding box of the face as well as the degree of confidence in the presence of a mask. As with prior object detection models, this model outputs a time-varying vector representing the spatial localization information for faces as  $J_m(t) = \{bb_{m1}(t), bb_{m2}(t), \dots, bb_{mk}(t), \dots, bb_{mn}(t)\}$ , where  $n$  is the number of face bounding boxes at time  $t$  and  $bb_{mk}(t) = (u, v, r, h, cm)$  is a five-tuple representation of the bounding box encompassing a detected face at time  $t$ . The variables  $u, v, r$ , and  $h$  have the same definitions as those in Section 2.1. The confidence measure  $c_m = (c_{mask}, c_{nomask})$  is a two-tuple in which  $c_{mask} \in [0, 1]$  indicates the probability of the presence of a mask and  $c_{nomask} \in [0, 1]$  indicates the absence. Similar to the Section 2.1, the tracking model returns a vector of the same size  $\overline{J}_m(t) = \{bbi_{p1}(t), bbi_{p2}(t), \dots, bbi_{pk}(t), \dots, bbi_{pn}(t)\}$  containing tracked bounding boxes for each  $t$ .

Similar to Section 2.1, the YOLO network was utilized for mask detection and the DeepSORT algorithm was utilized for tracking the masks across frames. The YOLO model was first initialized with the pre-trained COCO weights, and then fine-tuned using the images from the Moxa3k dataset [46] as well as the UT and UOP datasets which were labeled for mask detection. The DeepSORT model used the weights trained using the MOT dataset [59] for initialization.



(a) Bounding boxes for people and handshake



(b) Corresponding graph representation

Figure 4: Graph representation figure

## 2.6. Graph representation

The information extracted using different models in Section 2.1 - 2.5 need to be combined to provide meaningful insights on the threat level of the given scene. This is accomplished by encoding the data into a graph structure. This section describes how the graph structure is modelled using the different outputs from the models for interpretation.

The information retrieved from the video is stored as a time-varying graph  $G(t)$  given by,

$$G(t) = (V(t), E(t)) \quad (11)$$

and

$$V(t) = \{v_1(t), v_2(t), \dots, v_n(t)\} \quad (12)$$

$$E(t) = \{e_{1,1}(t), e_{1,2}(t), \dots, e_{i,j}(t), \dots, e_{n,n}(t)\} \quad (13)$$

where  $V(t)$  is the set of vertices and  $E(t)$  is the set of edges at time  $t$ . Each person  $P_i$  is denoted by a vertex  $v_i(t)$  which contains the features representing the person extracted from the video as time-varying vertex parameters. The vertex  $v_i(t)$  is given by,

$$v_i(t) = [location_i(t), mask_i(t), group_i(t)] \quad (14)$$

where  $location_i(t) = (x_i(t), y_i(t))$  is a two-tuple that represents the position of the person  $P_i$  at time  $t$  obtained through perspective transform to a bird's-eye view position on a 2D plane (refer Section 2.2).  $mask_i(t) = c_m$  is two-tuple which shows the confidence level that a person  $P_i$  is wearing a mask at time  $t$ . This information is extracted from  $bb_{mi}(t)$  depending on the index  $ID_{mi}(t)$  (refer Section 2.5).  $group_i(t)$  is a matrix that represents the probability that two people belong to the same group (refer Section 2.3). The edge  $e_{i,j}(t)$  is a binary value (0/1) that represents the presence (denoted by 1) or absence (denoted by 0) of an interaction between person  $P_i$  and  $P_j$  at time  $t$  (refer Section 2.4).  $E(t)$  is stored as a sparsely filled adjacency matrix with null values for instances where interactions are not detected.

## 2.7. Threat quantification

The information extracted from the models described in the proposed system in Sections 2.1 - 2.6 need to be processed from the created temporal graph in order to provide a quantifiable metric which denotes the risk of transmission for the given scene/video. In this section, the derivation of the threat level function which quantifies the threat of the given scene is described in detail.

Table 2 contains a list of the parameters that contribute to the spread of COVID-19. The parameters are divided into two categories: primary and secondary parameters, which will be discussed further in this section using the threat level function. The threat level  $T$  was calculated as follows for each frame at

time  $t$ ,

$$T(t) = \sum_{(v_1, v_2 \in V)} T_{v_1, v_2}(t) \quad (15)$$

$$T_{v_1, v_2}(t) = \sum_{p_i \in \mathbb{P}} p_i(v_1, v_2) \times \prod_{q_j \in \mathbb{Q}} \epsilon_j - q_j(v_1, v_2) \quad (16)$$

Table 2: Parameters used in threat quantification

Set	Notation	Description
$\mathbb{P}$	$p_d$	Distance between people
	$p_h$	Handshake interactions between people
$\mathbb{Q}$	$q_g$	People belonging to the same group
	$q_m$	People wearing masks

$\mathbb{P} = \{p_h, p_d\}$  is the set of parameters that directly attributes to the transmission of COVID-19 from one person to another. This includes the distance between people and the handshake interactions. As distance between people (people coming close) and their interactions (handshakes) play a primary role in the COVID-19 virus transmission, these values were first considered as the primary parameters  $\mathbb{P}$ . The probability of two people shaking hands  $p_h$  and the probability of them coming extremely close  $p_d$  were represented as scalar values in the range  $[0, 1]$ , where 1 represents a high probability of occurrence <sup>2</sup>.

$\mathbb{Q} = \{q_m, q_g\}$  is the set of secondary parameters which are relevant only when two people are in close proximity, and in such a case these parameters can increase or decrease the probability of COVID-19 transmission accordingly. This includes whether people are wearing masks since two people not wearing masks is irrelevant if they are far apart, and whether the persons belong to the same group. First, the mask-wearing probability  $q_m$  was used to quantify the effect of masks in transmission. Furthermore, people belonging to the same group ( $q_g$ ) have a similar effect on transmission, since it is assumed that the disease spread between them does not increase depending on what is happening in the video frame (it is more likely they were both infected or not, even before coming into the frame). The values of  $q_j$  are in the range  $[0, 1]$ .  $\epsilon_j \geq 1$  is used as a tuneable parameter which dictates the influence of a particular parameter  $q_j$  on the overall threat level. A higher  $\epsilon_j$  values give a lower significance to the corresponding  $q_j$  in calculating the total threat  $T(t)$ .

By substituting the parameters and setting  $\epsilon_m = 2.0$ ,  $\epsilon_g = 1.0$ , the equation was rewritten as follows,

$$T_{v_1, v_2}(t) = (p_h + p_d) (2.0 - q_m) (1.0 - q_g) \quad (17)$$

When analyzing the threat equation in Eq. (16), it can be noted that when the secondary parameter probabilities decrease (i.e.  $q_j$ ), the effect of the multiplicative term  $(\epsilon_j - q_j)$  is higher. This implies

<sup>2</sup>For the distance probability,  $1m$  is used as the threshold distance for being extremely close in this study

that, the effect of the primary parameters  $p_j$  to the threat of the given scene are compounded when the two persons have worsening secondary parameters (i.e. are not wearing masks or when they are of different groups). It can also be observed that (17) does not carry any terms with the  $p_d p_h$  product. This could be intuitively understood, because shaking hands require them to be physically close and thus, incorporating this term is redundant. While (17) is tuned for the implemented system, the generic form (16) can incorporate any number of parameters being extracted from a video scene.

### 3. Evaluation

In this section we discuss the methodology used to evaluate the system. The proposed solution was executed on a chosen set of datasets as the input and the results were evaluated using different metrics. The followings subsections describe the datasets, the metrics, and the evaluation execution process in detail.

#### 3.1. Datasets

To evaluate the performance of the individual components of the system (person detection, activity detection and mask recognition) existing datasets, MOT [56, 59, 60] and UT-interaction [61], were chosen. However, there are no existing datasets to perform a holistic analysis. Thus, in order to analyze handshake interactions, a new dataset was created from the University of ---text removed for double blind purposes--- premises which is referred to as the UOP dataset.

The **multiple object tracking (MOT)** datasets are a set of image sequences with annotations for people localization and people IDs. Three datasets [56, 59, 60] were used to evaluate the capability of an algorithm to uniquely identify and track a person through a video.

The **UT-interaction** dataset comprises of twenty video sequences of human interactions in a two or four people setting. The actions in the dataset include handshake, punch, point, kick, push and hug. Multiple scenes from the UT-interaction dataset [61, 62] were used to evaluate the capability of the handshake detection algorithm. For the purpose of action localisation, a ground truth for this dataset was created by annotating them since the original ground truth is a bounding box surrounding the two actors and not the action.

The **UOP dataset** is a collection of ten video sequences which were collected from the University of --text removed for double blind purposes-- premises by enacting a scene with human interactions. These videos were recorded by a wall-mounted CCTV camera in the university corridor and waiting area. The ground truth for this dataset was annotated manually for training and evaluation.

#### 3.2. Evaluation metrics

The outputs were evaluated on the given datasets based on two evaluation metrics namely, the average precision (AP) and the mean average precision (mAP). mAP is the key metric used in evaluating

detector performance in prominent object detection tasks such as PASCAL VOC challenge [63], COCO detection challenge [55] and the Google Open Images dataset competition [64].

The average precision (AP) is the precision value averaged across different recall values between 0 and 1 [65]. The AP is then calculated using Eq. (18). This was computed as the area under the curve (AUC) of the precision vs recall curve, plotted as a function of the confidence threshold of detection with a fixed intersection over union (IoU) for the bounding box threshold [66]. This IoU threshold is usually maintained at 0.5 in object detection tasks. For multi-class problems, the AP values for all class are averaged to obtain the Mean average precision (mAP) for the detector.

$$AP = \int_0^1 p(r)dr \quad (18)$$

### 3.3. Model evaluation

#### 3.3.1. People detection

The people detection component used here is of the YOLO network which is a well established detector. Hence, no modifications were introduced to this segment of the detector. The YOLOv4 model which was used here is extensively compared in terms of frame rate and mAP in [50]. The mAP value for YOLO’s performance is well established over 65%.

#### 3.3.2. Group identification

The group identification component was evaluated using the existing MOT datasets. Since the ground truth for the datasets considered in this work do not contain the group annotated information, an alternative methodology was required for evaluation. For this purpose, visual inspection of frames was used to determine if two individuals belonged to the same group in a given frame.

#### 3.3.3. Interaction detection

The evaluation of handshake interaction detection component requires the localization information of actions. However, the annotations of ground truth for the UT-interaction dataset focuses only the actors. Thus the UT-interaction dataset was re-annotated together with the UOP dataset, where 17 video sequences from the UT-interaction dataset and five videos from the UOP dataset were used for the training process.

The training phase of YOLO for handshake detection was done as follows. First, the YOLO model was pretrained on the Imagenet [67] dataset. Then it was fine-tuned to detect hands using the open images dataset [64]. This model was then retrained on the UOP dataset for handshakes using transfer learning to better the detection accuracy.

Since interaction detection is a single-class detection problem, the Average Precision (AP), which is the most versatile metric used in single-class object detection, was used for evaluation. A detection is considered true setting an IoU threshold of 0.5 or greater.

#### 3.3.4. Mask detection

Similar to interaction detection, the mask detection component requires localized information of masks. Thus, the UT-interaction dataset was re-annotated. However, this dataset only consists of unmasked faces, and as such the annotated UOP dataset was used together with the UT-interaction dataset to train and evaluate the mask detection component. The 17 videos from the UT-interaction dataset and the five videos from the UOP dataset were used for training. The dataset was annotated with the two class information, namely; masked and unmasked faces in frames, where the faces were visible and the presence of mask can be interpreted by a human.

The mask detection model was evaluated using both the AP and mAP measures. First, the models ability to localize the faces was determined by measuring the AP of the localization component of the models disregarding the class labels. The AP (average precision) was measured with a fixed IoU threshold of 0.5.

Next, the performance of the model in terms of both the localization and the accuracy was determined by the Mean Average Precision (mAP) value. Note that, since both the classes correspond to the same object (i.e. faces), this two-metric evaluation process helps us identify the specific shortcomings of the model considered. For instance, a high AP and a low mAP shows poor mask detection (classification), whereas a high accuracy and low mAP denotes poor face localization.

#### 3.3.5. Graph interpretation - Threat level quantification

The threat level quantification algorithm was tested on the three datasets mentioned earlier. Since there are no publicly available ground truth for videos for this parameter, the results of the algorithm were evaluated by comparison with expert human input. For this purpose, 462 samples of frame pairs from video sequences were chosen. The system was then evaluated by observing the increment/decrement of the inferred threat level  $T(t)$  and comparing the results with the expert human input. The performance of the full system is evaluated using accuracy, precision and recall.

The expert responses were obtained by showing a pair of frames and asking if the threat for COVID-19 spread has increased or decreased from the first frame to the second. Since a high disparity in identifying the impact of COVID-19 spread can exist amongst human experts in certain instances, a ground truth cannot be established for such pairs of frames. To identify such instances, a thresholding minimum majority required to establish ground truth was set as 70% and all frame pairs with a higher disparity (i.e. less than 70% majority) for any given choice (threat increased/decreased) were removed. In the evaluation conducted, five such frame pairs were identified and removed. One such frame pair is shown in Fig. 5 to conclude this factor. As it can be observed, it is difficult to assess the change in threat for COVID-19 spread (whether it increases or decreases) across these two frames.



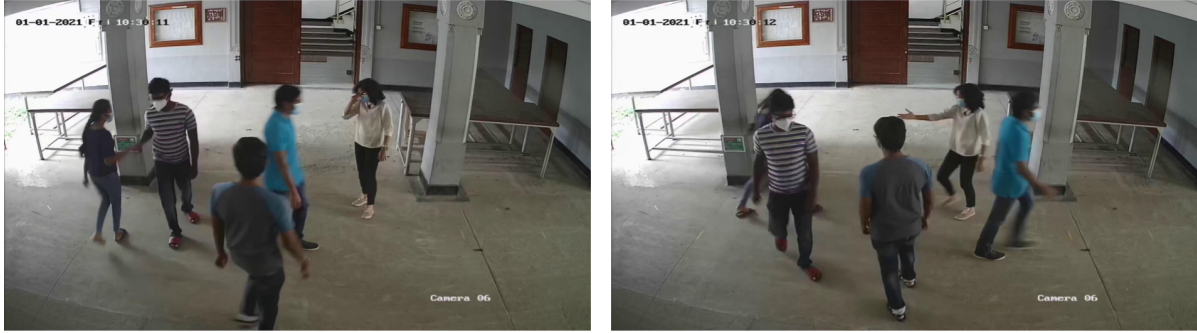


Figure 5: A pair of frames removed from full system evaluation due to disparity in human expert responses.

#### 4. Results and Discussion

The proposed system<sup>3</sup> was implemented using the Python programming language, and Tensorflow and OpenCV libraries. The system is deployed on a high performance computing server with NVIDIA GPU. The output of each component of the system as well as the final output of the entire system are discussed below.

##### 4.1. People detection and tracking



Figure 6: Results of people detection. Top row shows the cases where people detection model is successful. The bottom row shows instances where people detection is erroneous. Undetected people are marked by the purple oval. The green bounding box of the bottom row middle image does not span the full person.

The results shown in Fig. 6 are indicative of the performance of the human detection and tracking segment of the proposed system. The first row shows a sequence of frames where people are detected

<sup>3</sup>Code available at <https://github.com/pdncovid/covid-people-graph>

properly and tracked with unique IDs. However, the model fails to perform satisfactorily in specific scenarios. The bottom row gives examples for the cases the model can fail. From left, (1) a person is not being identified because of occlusion, (2) the identified bounding box is smaller than the person due to occlusion and (3) a person going undetected due to the lack of contrast with the background. The model has an mAP = 65% for the people detection task.

As observed in Fig. 6 a given frame from the output consists of multiple markings. The blue quadrilateral on the ground is the reference markings used for perspective transformation. The people detected are identified by uniquely colored rectangular bounding boxes. The location of each person in the 2D plane is marked using a black dot on the bottom edge of the respective bounding box. The threat level for the given frame is the numerical value displayed in the frame. Further details of the relevant markings will be discussed in the subsequent sections.

#### 4.2. Distance estimation

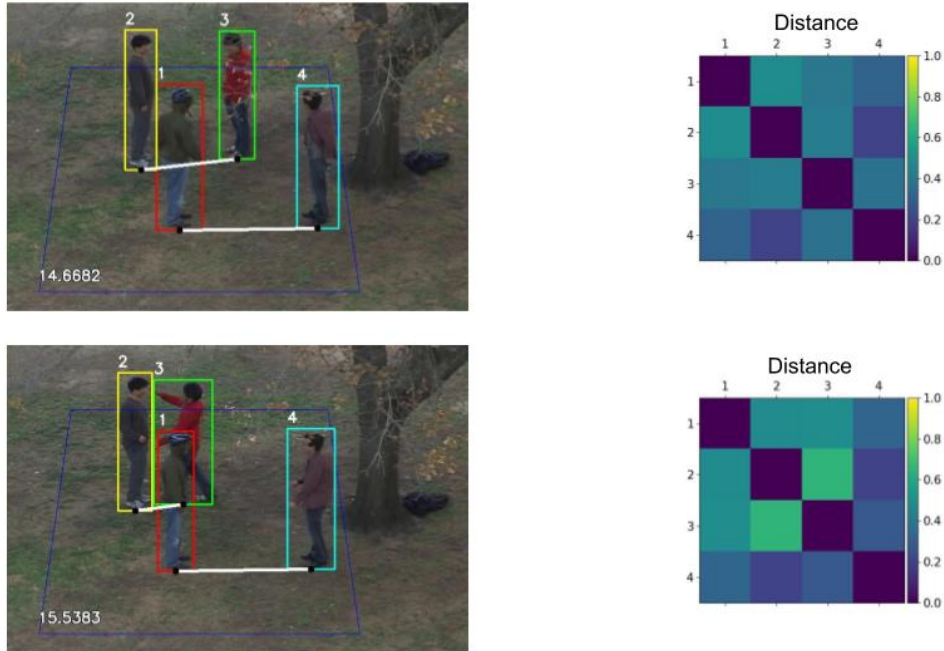


Figure 7: Distance results

A scene consisting of four people from UTI dataset is considered in Fig. 7 to show how distance between people contributes to the threat level. The distance between people is given by the distance activity matrix shown beside each frame in Fig. 7. Each element (square) in the activity matrix denotes the proximity between the person IDs corresponding to the row and column indices. The color changes to a warmer shade towards yellow when the people are closer, and becomes a colder shade towards blue when they are farther away.

Considering the frames in Fig. 7 the person ID 2 and 3 can be observed to be closer in the second frame than the first frame. This gives rise to a higher contribution to the threat level between them

in the second frame and a lower contribution to the threat level in the first frame. This is seen in the distance activity matrix by the blue shade turning to cyan indicating closer proximity between those persons. The reader’s attention is drawn to the threat level shown in each frame. As it can be observed, when the distance activity matrix lightens up, the threat level has also risen.

#### 4.3. Group identification

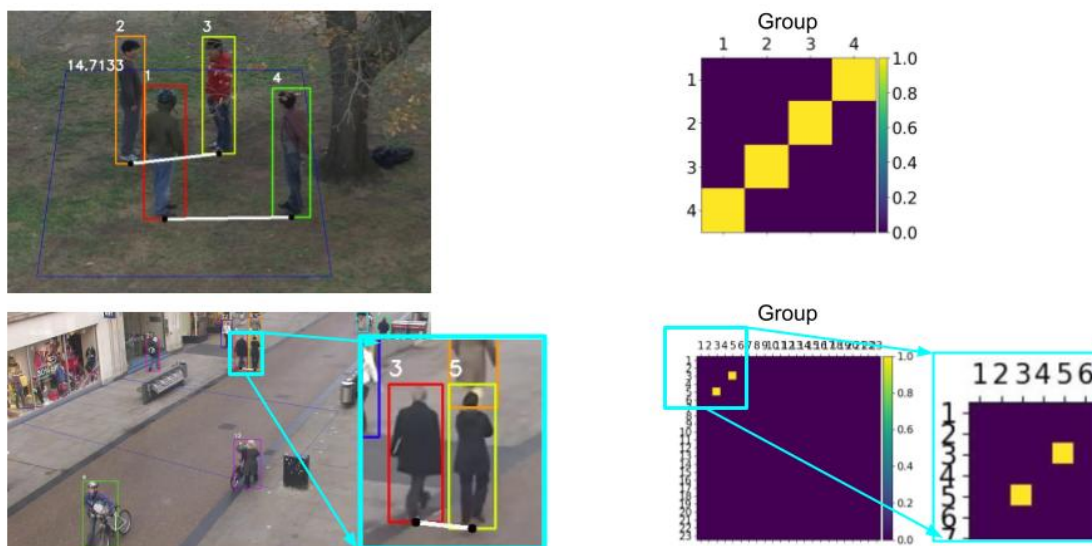


Figure 8: Group identification. Left: video frames where groups of people are denoted by white lines connecting individuals. Right: group activity matrices showing people belonging to the same group by yellow and else blue.

The results for a few frames for the group identification model is shown in Fig. 8. An example from the UTI dataset and Oxford towncenter datasets each is shown here. The frames with the persons detected is shown on the left and the group activity matrices showing the group characteristic is shown on the right. If two people are of the same group, the group activity matrix element corresponding to the row and column of the IDs of these two persons is shown in yellow and otherwise it is shown in blue. The people of the same group are also joined by a white line in the original frame to show this.

#### 4.4. Handshake detection

The performance of the system in detecting handshake interactions is shown in Fig. 9. Here two frames, one each from the UTI and UOP datasets are shown. The visualization of handshake interactions is the same as of the group activity matrices. The interaction activity matrix element corresponding to the row and column of the IDs of the two persons involved in the handshake is denoted by yellow, whereas if there is no handshake, it is depicted in blue. The handshake interaction detection and localization model performance is quantified by the AP evaluated on the UTI and UOP datasets separately and is tabulated in Table 3. The UTI dataset was tested on 3 videos with 418 frames and the UOP dataset

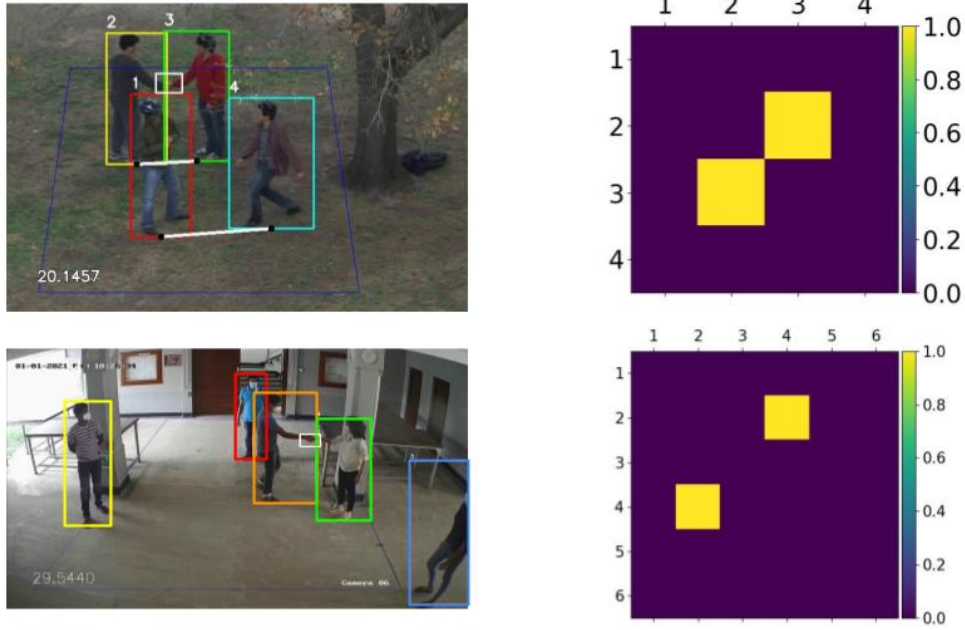


Figure 9: Handshake detection. Left: Sample frame denoting the detected people and white boxes denoting handshakes. Right: Group activity matrix.

was tested on 5 videos with 2786 frames. The precision vs recall curves for the UTI dataset and the UOP dataset are shown in Fig. 10. A detailed analysis of the results are given in [ ] (citation removed for double blind purposes).

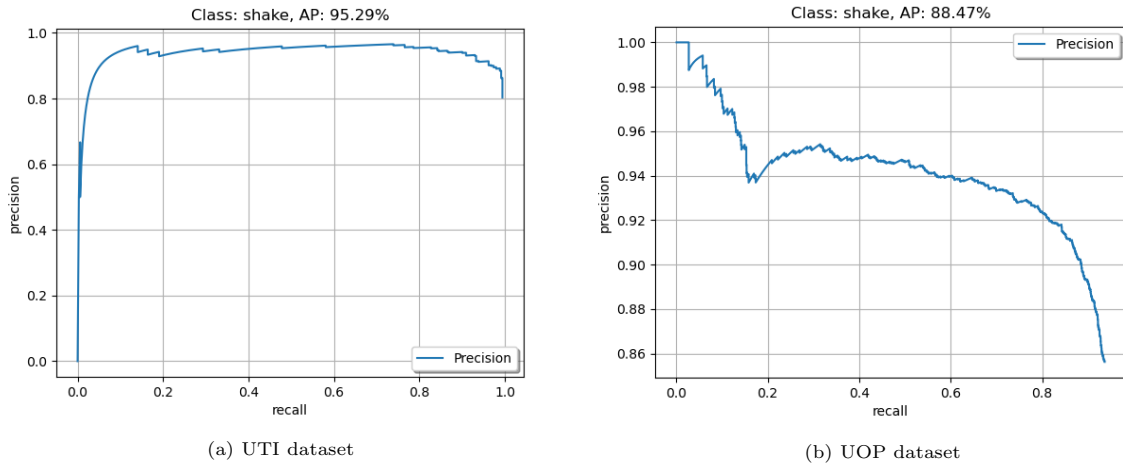


Figure 10: Precision vs Recall curves for handshake detector for UTI and UOP dataset.

Table 3: Performance metrics of handshake detection

Dataset	AP/%
UT-interaction	95.29
UOP	88.47

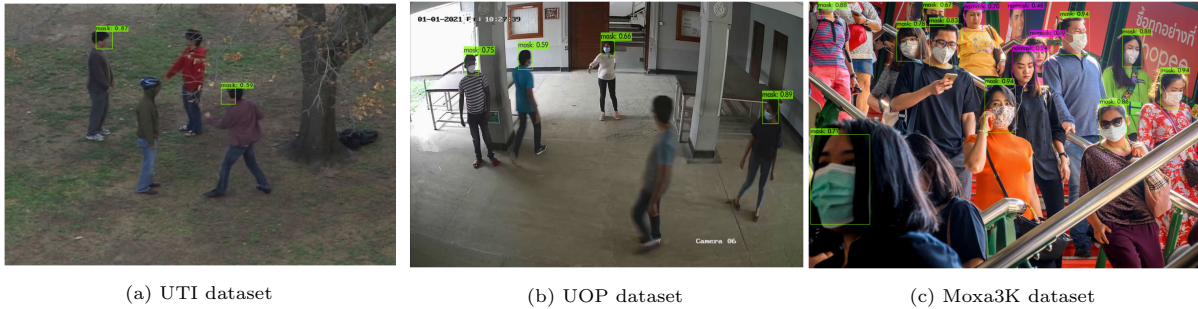


Figure 11: Mask detection detection examples.

#### 4.5. Mask detection

Fig. 11 shows the performance of the system in detecting the presence/absence of masks. One example from the UTI, UOP, and the Moxa3K datasets is shown. Overall the system perform well while dealing with high resolution images (Moxa3K). However, as the resolution drops (UTI / UOP), the efficacy reduces drastically. This can be observed from the Table 4 which lists the numerical evaluation metrics (AP and mAP) for localization on different datasets. We also note that the system performs significantly well in identifying masked faces, as opposed to unmasked faces.

Table 4: Performance metrics of the mask detection.

Dataset	AP/mAP /%
UT-interaction (Unmasked)	29.30
UOP (Masked)	41.47
Moxa3K	81.04

#### 4.6. Threat level assessment (end-to-end system)

To evaluate the proposed system performance, the threat level metric provided for each frame of a given scene is evaluated across multiple frames. The successful output of this value is evaluated by the full system for both datasets UTI (Figures 12, 13 and 14), and Oxford (Fig. 15). It should be noted that it is not the absolute values of the threat level that are significant but the increments or decrements between the frames.

Considering Figures 12, 13 and 14 it can be observed that the threat level increases from top to bottom frames as 14.7, 16.9 and 20.0. From the first frame to the second frame (Fig. 12 to Fig. 13), we can see the distance activity matrix brightening in the right top and left bottom edges. This is due to close proximity of persons ID 1 and 4. This leads to an increase in the threat level of the frame by  $16.9 - 14.7 = 2.2$ . Similarly, when looking at the first and third frames (Fig. 12 to Fig. 14), this time the interaction activity matrix brightens up in the third frame due to the handshake interaction in this frame. This also leads to an increase in threat level, which is by  $20.0 - 14.7 = 5.3$ . It is also clearly observed in the threat activity matrix for the third frame in Fig. 14, where the center squares brighten up to show a significant threat between person 2 and 3. This increment (of 5.3) in threat level is higher than the

previous comparison (of 2.2) in Fig. 12 and Fig. 13 since the handshake interaction poses a higher threat than proximity alone. The same can be observed by comparing the second and third frames.

A simpler situation is analyzed in Fig. 15. Here, there are only two people belonging to the same group and they are present in the video throughout the time. However, there are no physical interactions like shaking hands. Therefore, the only parameter that dictates the threat level is the number of people and their inter-personal distances in each frame. When analyzing the Fig. 15 the people in the first frame are moving away from each other until the second frame. This is why the threat level goes down from 95.0 to 46.0 from the first frame to the second. In the third frame, new people come into the frame and they get closer to each other. Therefore, an increase in the threat level of 105.3 is observed. However, this dataset does not contain a rich set of scenes to evaluate all components of the proposed system.

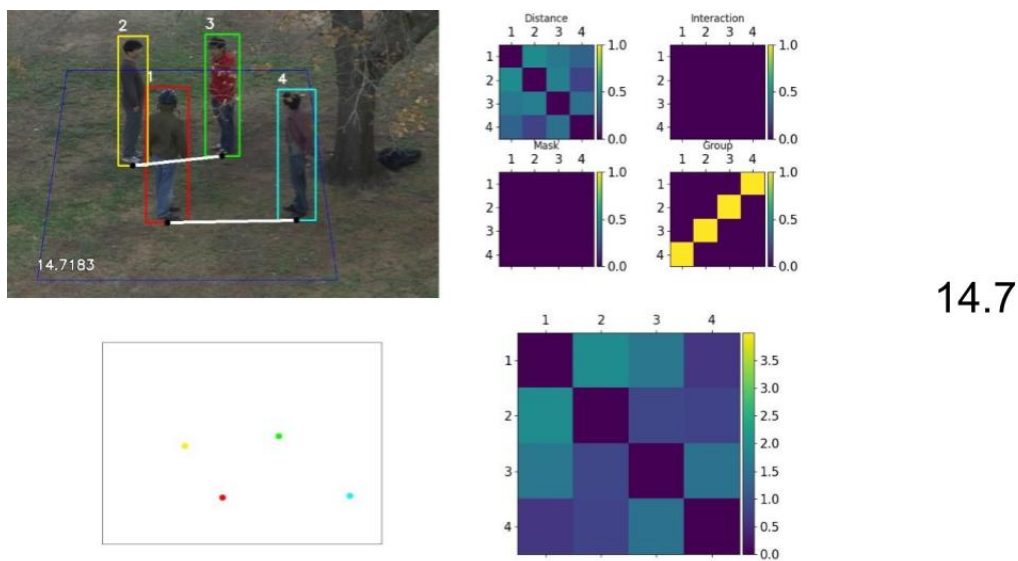


Figure 12: Full system result of UTI interaction dataset at  $t_1$

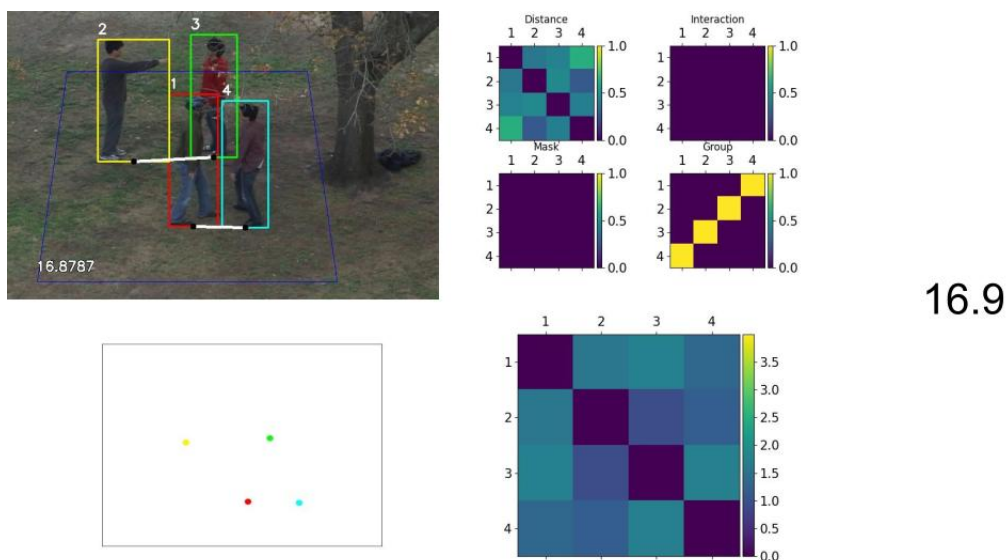


Figure 13: Full system result of UTI interaction dataset at  $t_2$

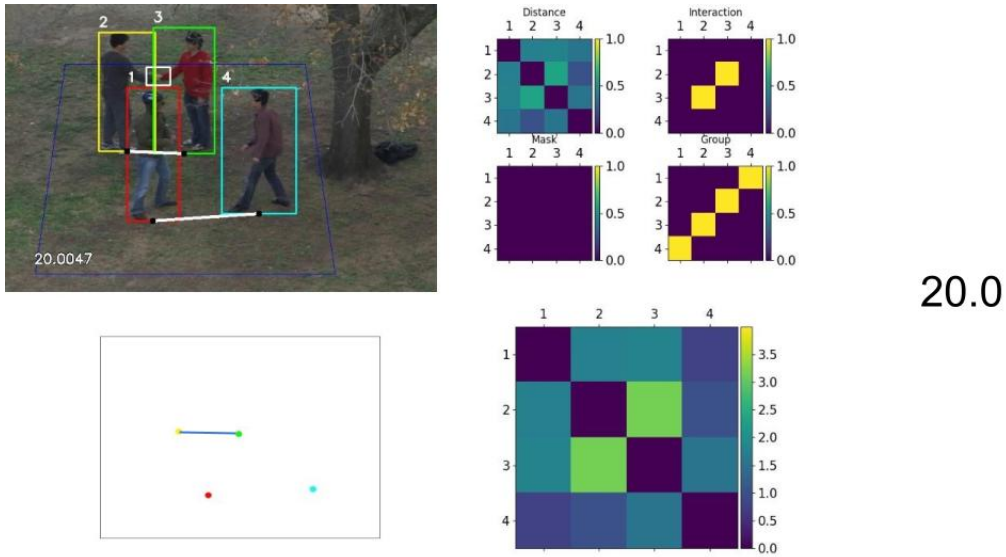


Figure 14: Full system result of UTI interaction dataset at  $t_3$

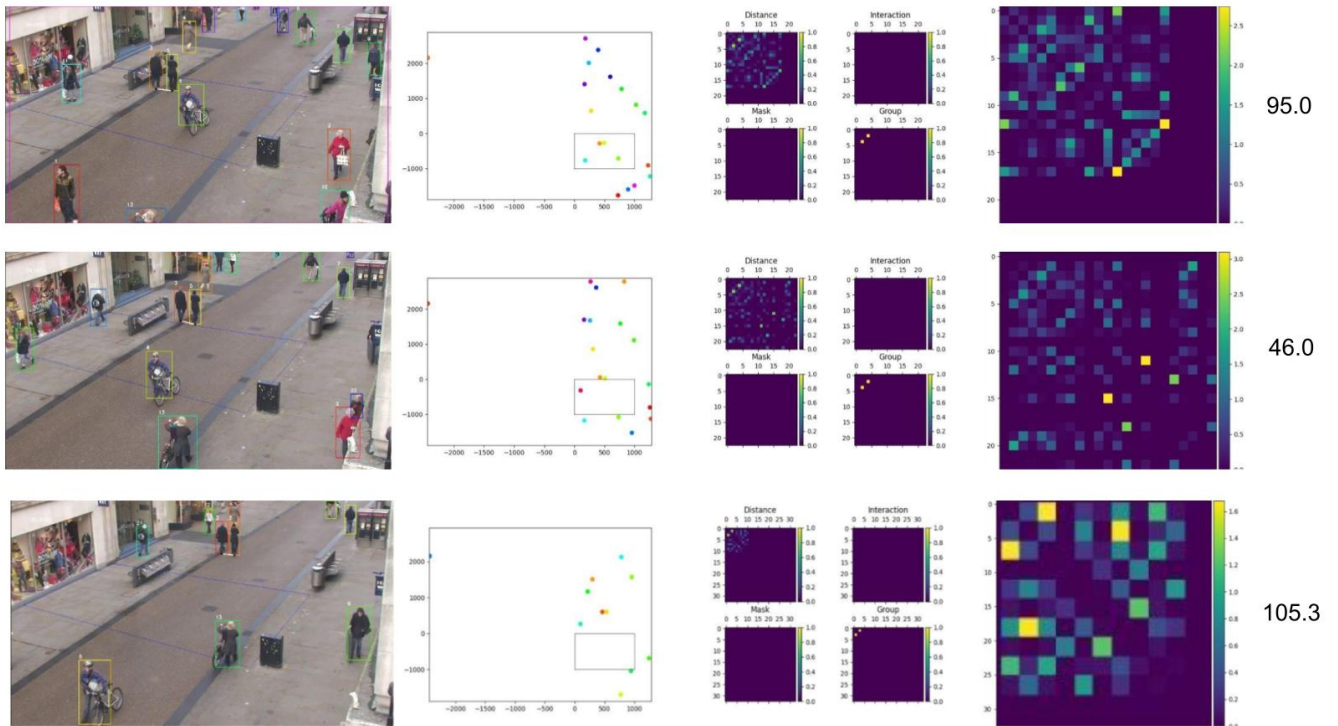


Figure 15: Full system result of oxford dataset

#### 4.7. Full system evaluation

The performance of the full system in comparison to human expert responses is provided in Table 5 in terms of accuracy, precision and recall. It can be noted that the system performance is not biased towards either dataset and is able to generalize with considerable accuracy of nearly 76%.

Few of the notable failure cases of the system are shown in Fig. 16 - 19, where the threat level

Table 5: Full system performance

Test	Accuracy	Precision	Recall
UTI dataset	75%	75%	75%
UOP dataset	76%	85%	79%
Overall	76%	81%	77%

predicted was on the contrary to human expert opinion. Out of the 4 cases shown here 3 of them failed to evaluate the proper threat value due to a failure in one of the components in the system pipeline. In Fig. 16, the person indicated by the purple arrow was not detected by the person detection model due to occlusion. Similarly, in Fig. 17 the two individuals hugging are detected as a single person. Since it is the proximity of the three individuals in Fig. 16 and the hugging individuals in Fig. 17 that pose a high threat to COVID-19 spread, the system fails to reflect this, deviating from the expert opinion. In Fig. 18 the high proximity of the individuals in the first frame give a high threat value for the first frame. However, the handshake interaction model fails to detect the interaction in the second frame hence leading to a lower threat level output by the system and hence failing to identify the increase in threat for COVID-19 spread. In the case of Fig. 19, since the system design was not accounted for incidents such as a pushing action as in the second frame, the system provides a higher threat value for the first frame on the contrary to human expert opinion.



Figure 16: Failure case 1 threat level interpretations  
System output for threat - Decreases, Human expert opinion on threat - Increases

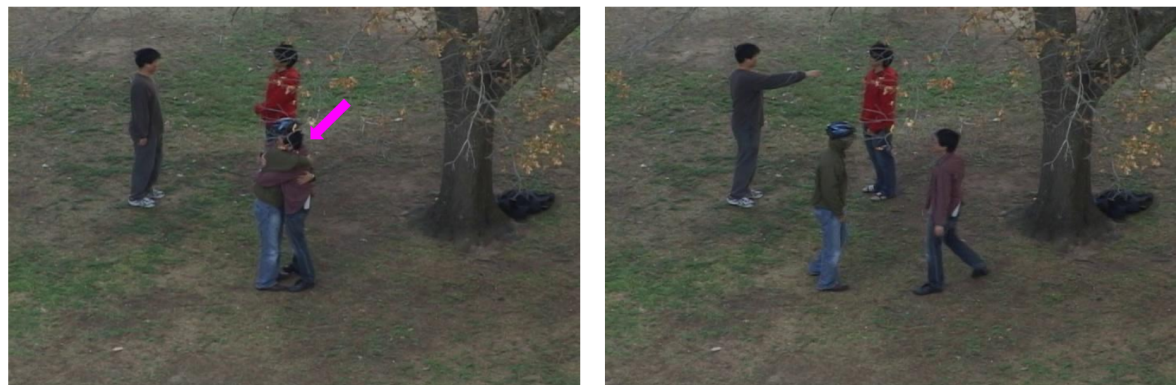


Figure 17: Failure case 2 threat level interpretations  
System output for threat - Increases, Human expert opinion on threat - Decreases





Figure 18: Failure case 3 threat level interpretations  
 System threat evaluation output - Decreases, Human expert opinion output - Increases



Figure 19: Failure case 4 threat level interpretations  
 System threat evaluation output - Decreases, Human expert opinion output - Increases

However, there were few rare cases where in retrospect, the system output was more plausible or instances where the failure by the system was unexplained. Considering Fig. 20, the ground truth from human expert opinion was that the threat level decreases, which is explained by the handshake interaction in the first frame which is a serious violation of social distancing protocols. However, the system output for threat value increases significantly in the second frame as a new person is identified in the far left. Since an increase in the number of people and closer proximity of this new person in a given space should also be accounted to, this leads to the increased threat value predicted by the system. In the meantime, Fig. 21 is an instance where the system output states the threat for COVID-19 spread has increased,

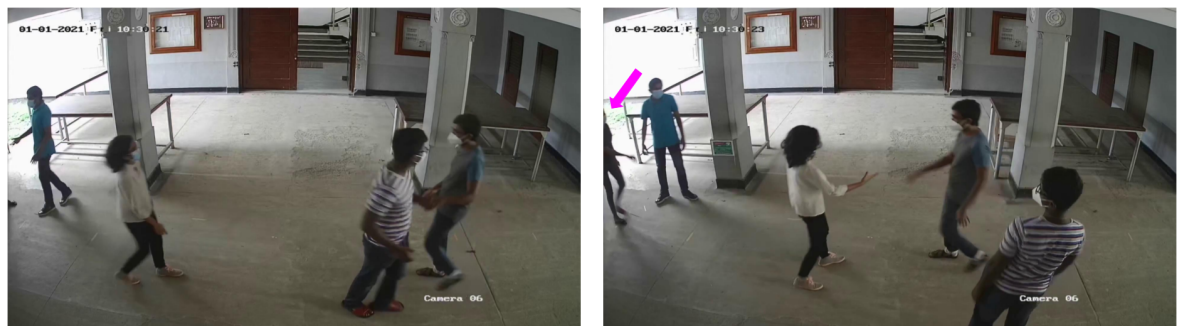


Figure 20: Edge case 1 threat level interpretations  
 System threat evaluation output - Increases, Human expert opinion output - Decreases



Figure 21: Edge case 2 threat level interpretations  
 System threat evaluation output - Increases, Human expert opinion output - Decreases

whereas human expert opinion is on the contrary. This deviation by the system is an edge case where the deviation is unexplained.

## 5. Conclusion

An end-to-end solution for monitoring social distancing protocols, interpersonal interactions such as handshakes, as well as mask-wearing; utilizing CCTV footage based on computer vision and graph theory is presented here. The proposed system provides a practical and versatile mechanism for monitoring crowds to identify possible instances for spreading COVID-19. The model was evaluated using pre-existing datasets as well as the proposed UOP dataset. Consistent accuracies over 75% across all datasets could be considered as a strong indication of the performance of the proposed system.

The proposed architecture and system enables it to identify violations of COVID-19 safety protocols, including social distancing and dyadic human interactions that are consistent with ground reality. This capability is enabled by the proposed system's holistic approach towards identifying the characteristics of crowd behavior and the behaviors of individuals within a crowd in a single frame as well as across multiple frames. In other words, it employs spatial and temporal analysis to ascertain critical properties such as the distance between individuals, mask-wearings, handshakes, and other interactions. This feature makes the proposed methodology more robust as typical human interactions (that may lead to the spread of COVID-19 or any other contagious disease) require close encounters of humans spanning some time duration. The proposed system realizes this characteristic.

Furthermore, this unified framework allows for future incorporation of possible other future measures for curtailing the spread of COVID-19 or any other epidemics impacting the health and safety of the society. Therefore, this proposed framework may be strengthened by incorporating additional COVID-19 specific features as well as it could be adapted and adopted for similar other scenarios that may benefit from video or CCTV based non-intrusive observations.

Due to the widespread use of CCTV cameras, the proposed system is applicable to a wide variety of real-world scenarios. The decreasing performance-to-cost ratio of computing hardware (capable of efficiently running ANN-based algorithms) has enabled even small organizations to acquire the system.

The release of the codebase as free and open source software (FOSS) can accelerate both third-party deployment and solution improvement. However, concerns about privacy, bias, and fairness in conducting analytics on people's CCTV footage should be addressed on an individual basis in accordance with the rules and regulations of individual organizations and countries.

### **Acknowledgements**

This work is funded by International Development Research Centre (IDRC), Canada and Lewis Power, Singapore. GPU computing resources were provided by NVIDIA to the Embedded Systems and Computer Architecture Laboratory (ESCAL), University of Peradeniya through the GPU donation program. This research was made possible through the University of Peradeniya research infrastructure funded by the residents of Sri Lanka through their contribution towards public education.

## References

- [1] Dahai Zhao, Feifei Yao, Lijie Wang, Ling Zheng, Yongjun Gao, Jun Ye, Feng Guo, Hui Zhao, and Rongbao Gao. A comparative study on the clinical features of coronavirus 2019 (covid-19) pneumonia with other pneumonias. *Clinical Infectious Diseases*, 71(15):756--761, 2020.
- [2] Brit Long, William J Brady, Alex Koyfman, and Michael Gottlieb. Cardiovascular complications in covid-19. *The American journal of emergency medicine*, 38(7):1504--1507, 2020.
- [3] Mark A Ellul, Laura Benjamin, Bhagteshwar Singh, Suzannah Lant, Benedict Daniel Michael, Ava Easton, Rachel Kneen, Sylviane Defres, Jim Sejvar, and Tom Solomon. Neurological associations of covid-19. *The Lancet Neurology*, 2020.
- [4] Jamie Lopez Bernal, Nick Andrews, Charlotte Gower, Eileen Gallagher, Ruth Simmons, Simon Thelwall, Julia Stowe, Elise Tessier, Natalie Groves, Gavin Dabrera, Richard Myers, Colin N.J. Campbell, Gayatri Amirthalingam, Matt Edmunds, Maria Zambon, Kevin E. Brown, Susan Hopkins, Meera Chand, and Mary Ramsay. Effectiveness of Covid-19 Vaccines against the B.1.617.2 (Delta) Variant. *New England Journal of Medicine*, 385(7):585--594, 2021.
- [5] Matthew McCallum, Jessica Bassi, Anna De Marco, Alex Chen, Alexandra C Walls, Julia Di Iulio, M Alejandra Tortorici, Mary-Jane Navarro, Chiara Silacci-Fregni, Christian Saliba, et al. SARS-CoV-2 immune evasion by variant B. 1.427/B. 1.429. *Science*, 373(6555):648--654, 2021.
- [6] Piero Olliaro, Els Torreale, and Michel Vaillant. Covid-19 vaccine efficacy and effectiveness—the elephant (not) in the room. *The Lancet Microbe*, 2(7):279--2809, 4 2021.
- [7] Ali Pormohammad, Mohammad Zarei, Saied Ghorbani, Mehdi Mohammadi, Mohammad Hossein Razizadeh, Diana L Turner, and Raymond J Turner. Efficacy and safety of covid-19 vaccines: A systematic review and meta-analysis of randomized clinical trials. *Vaccines*, 9(5):467, 2021.
- [8] Leila Abdullahi, John Joseph Onyango, Carol Mukiira, Joyce Wamicwe, Rachel Githiomi, David Kariuki, Cosmas Mugambi, Peter Wanjohi, George Githuka, Charles Nzioka, Jennifer Orwa, Rose Oronje, James Kariuki, and Lilian Mayieka. Community interventions in low—and middle-income countries to inform covid-19 control implementation decisions in kenya: A rapid systematic review. *PLOS ONE*, 15(12):1--29, 12 2020.
- [9] Swati Mukerjee, Clifton M. Chow, and Mingfei Li. Mitigation strategies and compliance in the covid-19 fight; how much compliance is enough? *PLOS ONE*, 16(8):1--19, 08 2021.
- [10] Swetaprovo Chaudhuri, Saptarshi Basu, Prasenjit Kabi, Vishnu R Unni, and Abhishek Saha. Modeling the role of respiratory droplets in covid-19 type pandemics. *Physics of Fluids*, 32(6):063309, 2020.

- [11] Thushara Galbadage, Brent M Peterson, and Richard S Gunasekera. Does covid-19 spread through droplets alone? *Frontiers in public health*, 8:163, 2020.
- [12] Trisha Greenhalgh, Jose L Jimenez, Kimberly A Prather, Zeynep Tufekci, David Fisman, and Robert Schooley. Ten scientific reasons in support of airborne transmission of sars-cov-2. *The lancet*, 397(10285):1603--1605, 2021.
- [13] Derek K Chu, Elie A Akl, Stephanie Duda, Karla Solo, Sally Yaacoub, Holger J Schünemann, Amena El-harakeh, Antonio Bognanni, Tamara Lotfi, Mark Loeb, et al. Physical distancing, face masks, and eye protection to prevent person-to-person transmission of sars-cov-2 and covid-19: a systematic review and meta-analysis. *The lancet*, 395(10242):1973--1987, 2020.
- [14] Nina B Masters, Shu-Fang Shih, Allen Bukoff, Kaitlyn B Akel, Lindsay C Kobayashi, Alison L Miller, Harapan Harapan, Yihan Lu, and Abram L Wagner. Social distancing in response to the novel coronavirus (covid-19) in the united states. *PloS one*, 15(9):e0239025, 2020.
- [15] Linda Thunström, Stephen C Newbold, David Finnoff, Madison Ashworth, and Jason F Shogren. The benefits and costs of using social distancing to flatten the curve for covid-19. *Journal of Benefit-Cost Analysis*, 11(2):179--195, 2020.
- [16] Günter Kampf. Potential role of inanimate surfaces for the spread of coronaviruses and their inactivation with disinfectant agents. *Infection Prevention in Practice*, 2(2):100044, 2020.
- [17] Sarah L Warnes, Zoë R Little, and C William Keevil. Human coronavirus 229e remains infectious on common touch surface materials. *MBio*, 6(6), 2015.
- [18] Steffen E Eikenberry, Marina Mancuso, Enahoro Iboi, Tin Phan, Keenan Eikenberry, Yang Kuang, Eric Kostelich, and Abba B Gumel. To mask or not to mask: Modeling the potential for face mask use by the general public to curtail the covid-19 pandemic. *Infectious Disease Modelling*, 5:293--308, 2020.
- [19] Shakil Bin Kashem, Dwayne M Baker, Silvia R González, and C Aujean Lee. Exploring the nexus between social vulnerability, built environment, and the prevalence of covid-19: A case study of chicago. *Sustainable cities and society*, 75:103261, 2021.
- [20] Hassan Ugail, Riya Aggarwal, Andrés Iglesias, Newton Howard, Almudena Campuzano, Patricia Suárez, Muazzam Maqsood, Farhan Aadil, Irfan Mehmood, Sarah Gleghorn, et al. Social distancing enhanced automated optimal design of physical spaces in the wake of the covid-19 pandemic. *Sustainable Cities and Society*, 68:102791, 2021.

- [21] Chen Ren, Chang Xi, Junqi Wang, Zhuangbo Feng, Fuzhan Nasiri, Shi-Jie Cao, and Fariborz Haghighat. Mitigating covid-19 infection disease transmission in indoor environment using physical barriers. *Sustainable cities and society*, 74:103175, 2021.
- [22] Shubham Srivastava, Xingwang Zhao, Ati Manay, and Qingyan Chen. Effective ventilation and air disinfection system for reducing coronavirus disease 2019 (covid-19) infection risk in office buildings. *Sustainable Cities and Society*, page 103408, 2021.
- [23] George Grekousis and Ye Liu. Digital contact tracing, community uptake, and proximity awareness technology to fight covid-19: a systematic review. *Sustainable cities and society*, 71:102995, 2021.
- [24] Sizhen Bian, Bo Zhou, Hymalai Bello, and Paul Lukowicz. A wearable magnetic field based proximity sensing system for monitoring covid-19 social distancing. In *Proceedings of the 2020 International Symposium on Wearable Computers*, pages 22--26, 2020.
- [25] Maria Fazio, Alina Buzachis, Antonino Galletta, Antonio Celesti, and Massimo Villari. A proximity-based indoor navigation system tackling the COVID-19 social distancing measures. *Proceedings - IEEE Symposium on Computers and Communications*, 2020-July, 2020.
- [26] Ross Girshick. Fast r-cnn. In *Proceedings of the IEEE international conference on computer vision*, pages 1440--1448, 2015.
- [27] Wei Liu, Dragomir Anguelov, Dumitru Erhan, Christian Szegedy, Scott Reed, Cheng-Yang Fu, and Alexander C Berg. Ssd: Single shot multibox detector. In *European conference on computer vision*, pages 21--37. Springer, 2016.
- [28] Mohammad Javad Shafiee, Brendan Chywyl, Francis Li, and Alexander Wong. Fast yolo: A fast you only look once system for real-time embedded object detection in video. *arXiv preprint arXiv:1709.05943*, 2017.
- [29] Rafael Munoz-Salinas, Eugenio Aguirre, and Miguel García-Silvente. People detection and tracking using stereo vision and color. *Image and Vision Computing*, 25(6):995--1007, 2007.
- [30] Jacek Czyz, Branko Ristic, and Benoit Macq. A particle filter for joint detection and tracking of color objects. *Image and Vision Computing*, 25(8):1271--1281, 2007.
- [31] Nicolai Wojke, Alex Bewley, and Dietrich Paulus. Simple online and realtime tracking with a deep association metric. *Proceedings - International Conference on Image Processing, ICIP*, 2017-Sept:3645--3649, 2018.
- [32] N. Wojke, A. Bewley, and D. Paulus. Simple online and realtime tracking with a deep association metric. In *2017 IEEE International Conference on Image Processing (ICIP)*, pages 3645--3649, 2017.

- [33] Rung-Ching Chen et al. Automatic license plate recognition via sliding-window darknet-yolo deep learning. *Image and Vision Computing*, 87:47--56, 2019.
- [34] Xing-Yu Ye, Dza-Shiang Hong, Hung-Hao Chen, Pei-Yung Hsiao, and Li-Chen Fu. A two-stage real-time yolov2-based road marking detector with lightweight spatial transformation-invariant classification. *Image and Vision Computing*, 102:103978, 2020.
- [35] Sheng-Ho Chiang, Tsaipei Wang, and Yi-Fu Chen. Efficient pedestrian detection in top-view fisheye images using compositions of perspective view patches. *Image and Vision Computing*, 105:104069, 2021.
- [36] Dihua Wu, Shuaichao Lv, Mei Jiang, and Huaibo Song. Using channel pruning-based yolo v4 deep learning algorithm for the real-time and accurate detection of apple flowers in natural environments. *Computers and Electronics in Agriculture*, 178:105742, 2020.
- [37] Mohd Aquib Ansari and Dushyant Kumar Singh. Monitoring social distancing through human detection for preventing/reducing covid spread. *International Journal of Information Technology*, pages 1--10, 2021.
- [38] Imran Ahmed, Misbah Ahmad, and Gwanggil Jeon. Social distance monitoring framework using deep learning architecture to control infection transmission of covid-19 pandemic. *Sustainable Cities and Society*, 69:102777, 2021.
- [39] Imran Ahmed, Misbah Ahmad, Joel JPC Rodrigues, Gwanggil Jeon, and Sadia Din. A deep learning-based social distance monitoring framework for covid-19. *Sustainable Cities and Society*, 65:102571, 2021.
- [40] Jingchen Qin and Ning Xu. Reaserch and implementation of social distancing monitoring technology based on ssd. *Procedia Computer Science*, 183:768--775, 2021.
- [41] Adina Rahim, Ayesha Maqbool, and Tauseef Rana. Monitoring social distancing under various low light conditions with deep learning and a single motionless time of flight camera. *Plos one*, 16(2):e0247440, 2021.
- [42] Jie Su, Xiaohai He, Linbo Qing, Tong Niu, Yongqiang Cheng, and Yonghong Peng. A novel social distancing analysis in urban public space: A new online spatio-temporal trajectory approach. *Sustainable Cities and Society*, 68:102765, 2021.
- [43] Mahdi Rezaei and Mohsen Azarmi. Deepsocial: Social distancing monitoring and infection risk assessment in covid-19 pandemic. *Applied Sciences (Switzerland)*, 10(21):1--29, 2020.

- [44] Dongfang Yang, Ekim Yurtsever, Vishnu Renganathan, Keith A Redmill, and Ümit Özgüner. A vision-based social distancing and critical density detection system for covid-19. *Sensors*, 21(13):4608, 2021.
- [45] Narinder Singh Punn, Sanjay Kumar Sonbhadra, and Sonali Agarwal. Monitoring COVID-19 social distancing with person detection and tracking via fine-tuned YOLO v3 and Deepsort techniques, 2020.
- [46] Biparnak Roy, Subhadip Nandy, Debojit Ghosh, Debarghya Dutta, Pritam Biswas, and Tamodip Das. Moxa: a deep learning based unmanned approach for real-time monitoring of people wearing medical masks. *Transactions of the Indian National Academy of Engineering*, 5(3):509–518, 2020.
- [47] Puranjay Mohan, Aditya Jyoti Paul, and Abhay Chirania. A tiny cnn architecture for medical face mask detection for resource-constrained endpoints. In *Innovations in Electrical and Electronic Engineering*, pages 657–670. Springer, 2021.
- [48] Mohamed Loey, Gunasekaran Manogaran, Mohamed Hamed N Taha, and Nour Eldeen M Khalifa. Fighting against covid-19: A novel deep learning model based on yolo-v2 with resnet-50 for medical face mask detection. *Sustainable cities and society*, 65:102600, 2021.
- [49] Peishu Wu, Han Li, Nianyin Zeng, and Fengping Li. Fmd-yolo: An efficient face mask detection method for covid-19 prevention and control in public. *Image and Vision Computing*, 117:104341, 2022.
- [50] Shubham Shinde, Ashwin Kothari, and Vikram Gupta. Yolo based human action recognition and localization. *Procedia computer science*, 133:831–838, 2018.
- [51] Yasaman S Sefidgar, Arash Vahdat, Stephen Se, and Greg Mori. Discriminative key-component models for interaction detection and recognition. *Computer Vision and Image Understanding*, 135:16–30, 2015.
- [52] Coert Van Gemeren, Ronald Poppe, and Remco C Veltkamp. Hands-on: deformable pose and motion models for spatiotemporal localization of fine-grained dyadic interactions. *EURASIP Journal on Image and Video Processing*, 2018(1):1–16, 2018.
- [53] Alexey Bochkovskiy, Chien-Yao Wang, and Hong-Yuan Mark Liao. Yolov4: Optimal speed and accuracy of object detection, 2020.
- [54] John Canny. A computational approach to edge detection. *IEEE Transactions on pattern analysis and machine intelligence*, (6):679–698, 1986.



- [55] Tsung-Yi Lin, Michael Maire, Serge Belongie, James Hays, Pietro Perona, Deva Ramanan, Piotr Dollár, and C Lawrence Zitnick. Microsoft coco: Common objects in context. In *European conference on computer vision*, pages 740–755. Springer, 2014.
- [56] Patrick Dendorfer, Hamid Rezaatofghi, Anton Milan, Javen Shi, Daniel Cremers, Ian Reid, Stefan Roth, Konrad Schindler, and Laura Leal-Taixé. Mot20: A benchmark for multi object tracking in crowded scenes. *arXiv preprint arXiv:2003.09003*, 2020.
- [57] Yan Jiang, Feng Gao, and Guoyan Xu. Computer vision-based multiple-lane detection on straight road and in a curve. In *2010 International Conference on Image Analysis and Signal Processing*, pages 114–117. IEEE, 2010.
- [58] Ulrike Von Luxburg. A tutorial on spectral clustering. *Statistics and computing*, 17(4):395–416, 2007.
- [59] Anton Milan, Laura Leal-Taixé, Ian Reid, Stefan Roth, and Konrad Schindler. Mot16: A benchmark for multi-object tracking. *arXiv preprint arXiv:1603.00831*, 2016.
- [60] Laura Leal-Taixé, Anton Milan, Ian Reid, Stefan Roth, and Konrad Schindler. Motchallenge 2015: Towards a benchmark for multi-target tracking. *arXiv preprint arXiv:1504.01942*, 2015.
- [61] M. S. Ryoo and J. K. Aggarwal. UT-Interaction Dataset, ICPR contest on Semantic Description of Human Activities (SDHA). [http://cvrc.ece.utexas.edu/SDHA2010/Human\\_Interaction.html](http://cvrc.ece.utexas.edu/SDHA2010/Human_Interaction.html), 2010.
- [62] M. S. Ryoo and J. K. Aggarwal. Spatio-temporal relationship match: Video structure comparison for recognition of complex human activities. In *IEEE International Conference on Computer Vision (ICCV)*, 2009.
- [63] Mark Everingham, Luc Van Gool, Christopher KI Williams, John Winn, and Andrew Zisserman. The pascal visual object classes (voc) challenge. *International journal of computer vision*, 88(2):303–338, 2010.
- [64] Alina Kuznetsova, Hassan Rom, Neil Alldrin, Jasper Uijlings, Ivan Krasin, Jordi Pont-Tuset, Shahab Kamali, Stefan Popov, Matteo Mallocci, Alexander Kolesnikov, et al. The open images dataset v4: Unified image classification, object detection, and visual relationship detection at scale. *arXiv preprint arXiv:1811.00982*, 2018.
- [65] Stephen Robertson. A new interpretation of average precision. In *Proceedings of the 31st annual international ACM SIGIR conference on Research and development in information retrieval*, pages 689–690, 2008.

- [66] R. Padilla, S. L. Netto, and E. A. B. da Silva. A survey on performance metrics for object-detection algorithms. In *2020 International Conference on Systems, Signals and Image Processing (IWSSIP)*, pages 237--242, 2020.
- [67] Jia Deng, Wei Dong, Richard Socher, Li-Jia Li, Kai Li, and Li Fei-Fei. Imagenet: A large-scale hierarchical image database. In *2009 IEEE conference on computer vision and pattern recognition*, pages 248--255. Ieee, 2009.